Article

Current Biology

Inhomogeneous Encoding of the Visual Field in the Mouse Retina

Graphical Abstract

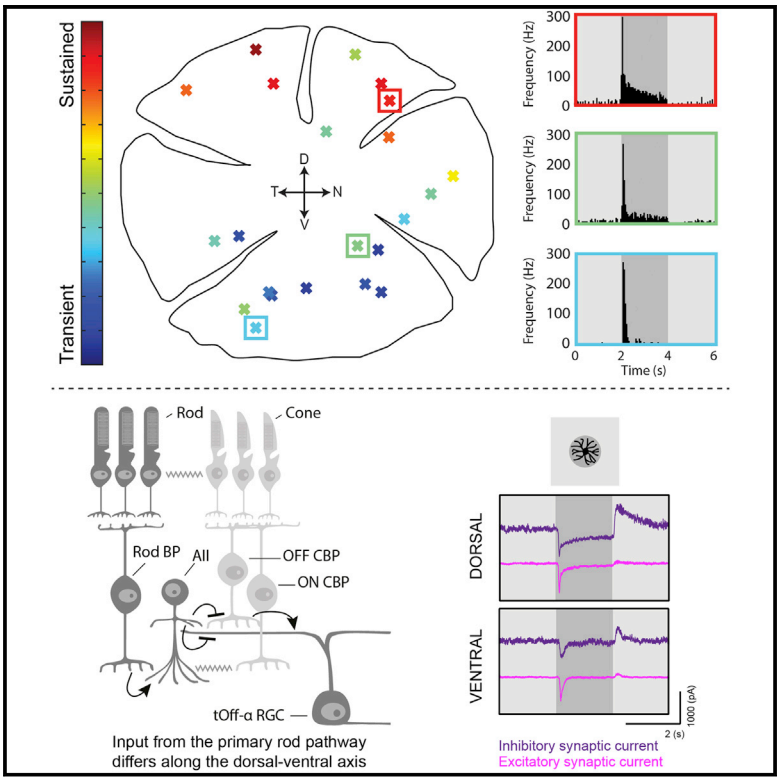

Highlights

- tOffα-RGCs become more sustained along the ventral-dorsal retinal axis
- Synaptic input from the primary rod pathway underlies these differences
- Similar differences are detected in transgenic mice and in wild house mice
- Location matters when studying visually related neuronal activity

Authors

Rebekah A. Warwick, Nathali Kaushansky, Nimrod Sarid, Amir Golan, Michal Rivlin-Etzion

Correspondence

michal.rivlin@weizmann.ac.il

In Brief

Warwick et al. show that retinal ganglion cells of the same subtype display different light responses depending on retinal location, resulting from variations in their underlying circuits. They suggest that these variations enable optimized sampling of the visual image.

Warwick et al., 2018, Current Biology *28*, 1–11
March 5, 2018
https://doi.org/10.1016/j.cub.2018.01.016

CellPress

Please cite this article in press as: Warwick et al., Inhomogeneous Encoding of the Visual Field in the Mouse Retina, Current Biology (2018), https://doi.org/10.1016/j.cub.2018.01.016

Current Biology
Article

Inhomogeneous Encoding of the Visual Field in the Mouse Retina

Rebekah A. Warwick,[1] Nathali Kaushansky,[1] Nimrod Sarid,[1] Amir Golan,[1] and Michal Rivlin-Etzion[1,2,*]
[1]Department of Neurobiology, Weizmann Institute of Science, 234 Herzl Street, Rehovot 7610001, Israel
[2]Lead Contact
*Correspondence: michal.rivlin@weizmann.ac.il
https://doi.org/10.1016/j.cub.2018.01.016

SUMMARY

Stimulus characteristics of the mouse's visual field differ above and below the skyline. Here, we show for the first time that retinal ganglion cells (RGCs), the output neurons of the retina, gradually change their functional properties along the ventral-dorsal axis to allow better representation of the different stimulus characteristics. We conducted two-photon targeted recordings of transient-Offα-RGCs and found that they gradually became more sustained along the ventral-dorsal axis, revealing >5-fold-longer duration responses in the dorsal retina. Using voltage-clamp recordings, pharmacology, and genetic manipulation, we demonstrated that the primary rod pathway underlies this variance. Our findings challenge the current belief that RGCs of the same subtype exhibit the same light responses, regardless of retinal location, and suggest that networks underlying RGC responses may change with retinal location to enable optimized sampling of the visual image.

INTRODUCTION

Visual processing begins in the retina, where the photoreceptors' signal is transferred to a diverse set of retinal cells that split the information into multiple channels carried by retinal ganglion cells (RGCs), the output neurons of the retina [1–3]. RGCs are composed of multiple subtypes, each of which encodes a specific modality in the visual field. Conventionally, RGC subtype classification relies on three criteria. First, RGCs belonging to a single subtype share the same light responses. Classical physiological characterizations of RGCs are based on the cells' responses to changes in illumination and define the cells as either On (respond to light increments), Off (respond to light decrements), or On-Off, and as either transient or sustained based on their response durations [4]. Further classifications are made based on the cells' responses to specific stimuli, such as direction selectivity or local edge detection [5–10]. Second, RGCs of the same subtype have similar morphological characteristics, sharing the same dendritic stratification layer within the inner plexiform layer; in species, such as mouse, that bear no fovea or area centralis, RGCs of the same subtype also have similar soma size and dendritic area [11, 12]. Third, as each RGC subtype acts as a channel reporting on a specific visual modality, a given RGC subtype tiles the retina in a mosaic-like fashion to represent the visual modality over the entire visual field [13–15].

This classification of RGCs assumes that all cells belonging to a single RGC subtype are alike, regardless of retinal location. However, the properties of the mouse visual scene differ between the lower and upper fields. Whereas the lower visual field, imaged by the dorsal retina, often detects the ground, the upper visual field, imaged by the ventral retina, frequently detects the sky. Indeed, natural visual scenes are known to have different spectral compositions and contrast distribution in the two domains divided by the horizon [16, 17]. This suggests that retinal neurons may display non-uniform properties across the retina, adapting to the prevalent signals to which they are exposed. Indeed, mouse photoreceptors show asymmetric distribution of S opsin (short-wavelength or UV light sensitive) and M opsin (mid-wavelength or green light sensitive) along the dorsal-ventral axis [18–20]. The asymmetric distribution was found to improve sampling of natural achromatic contrasts in cone photoreceptors and to generate differential chromatic response properties in RGCs [19, 21].

Here, we tested whether, on top of this opsin expression asymmetry, RGCs belonging to a single subtype display different light responses that are inherent to their underlying circuits. For this purpose, we took advantage of a well-characterized transgenic mouse line in which transient Off-alpha RGCs (tOff-αRGCs) are fluorescently labeled with GFP [22] and carried out two-photon targeted recordings. We found that the response properties of tOff-αRGCs differ with their location along the dorsal-ventral axis. While ventrally located cells display transient responses to light decrement (as their name indicates), dorsally located cells display comparably sustained responses to light decrement. This functional difference arose from their underlying circuitry, with cells in the dorsal retina receiving greater input from the primary rod pathway than cells in the ventral retina. These data demonstrate for the first time that cells belonging to a specific RGC subtype and sharing similar morphology may display different light responses as a function of their location within the retina. We hypothesize that RGCs adjust their response properties with retinal location to better represent the prevalent visual input that they encounter.

RESULTS

Transient Off-α RGCs Are More Sustained in the Dorsal Retina Compared with the Ventral Retina

In order to understand whether RGCs have uniform response properties across the retina, we investigated the light

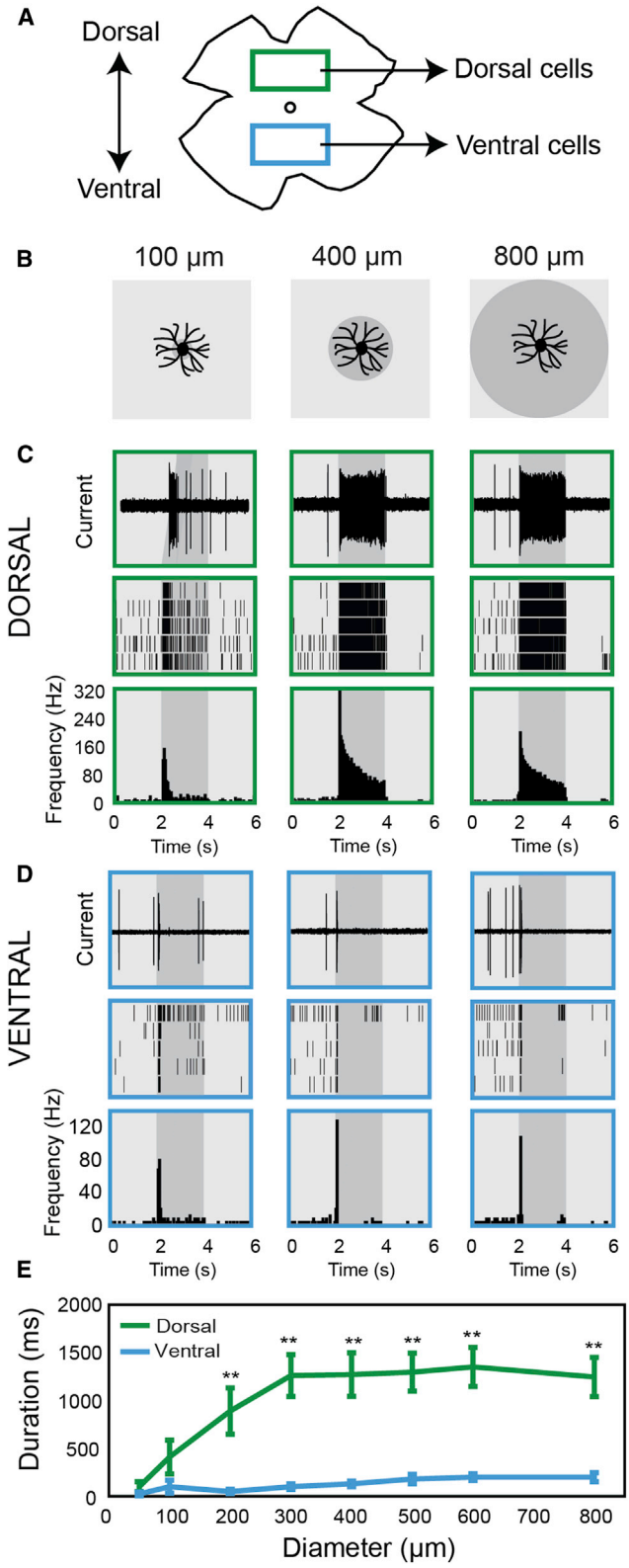

Figure 1. Dorsal tOff-αRGCs Have Longer Duration Responses Compared with Ventral tOff-αRGCs

(A) Diagram illustrating the two different areas of the retina from which dorsal- and ventral-tOff-αRGCs were recorded.

(B) Diagram illustrating some of the light stimuli.

(C and D) Examples of firing patterns from a dorsal-tOff-αRGC (C) and a ventral-tOff-αRGC (D). Top: example traces for the different corresponding spot sizes shown in (B). Middle: raster plots showing the spiking activity to the different sized spots for 5 repeat trials. Bottom: peri-stimulus time histograms (PSTHs) of the cell's responses calculated across 5 trails.

(E) Response duration as a function of spot size for dorsal- (green) and ventral- (blue) tOff-αRGCs. Error bars represent the mean ± SEM; n = 10 cells for each group. **p < 0.01; spot-size-based comparisons between dorsal- and ventral-tOff-αRGCs according to Wilcoxon rank-sum test.

See also Figures S1 and S2.

responses of tOff-αRGCs located either in the central dorsal area or the central ventral area of the retina (Figure 1A). For this purpose, we carried out two-photon targeted cell attached recordings in retinas of the transgenic mouse line, *Calb2-EGFP*, which selectively expresses GFP in one subtype of RGCs, the tOff-αRGCs [22]. The light stimulus was in the photopic range and consisted of a dark spot centered on the cell soma, appearing for 2 s on a gray background (Figure 1B; see STAR Methods). In order to examine the receptive field properties, a variety of spot sizes were used, ranging from 50 to 800 µm in diameter (Figure 1B).

We compared the responses of tOff-αRGCs located in the dorsal retina to the responses of tOff-αRGCs located in the ventral retina, which we term as dorsal-tOff-αRGCs and ventral-tOff-αRGCs, respectively. We calculated the total length of time the cells responded significantly to the black spot stimulus, which we refer to as the response duration. Unexpectedly, dorsal-tOff-αRGCs had significantly longer response durations than ventral-tOff-αRGCs (Figures 1C–1E, S1A, and S1B). The duration of the response in dorsal-tOff-αRGCs increased with increasing spot size and then plateaued for spot sizes larger than 300 µm in diameter, corresponding to the size of their dendritic tree and indicating little surround effect [11, 23, 24] (Figure 1E). The duration of the response in ventral-tOff-αRGCs was significantly shorter and independent of spot size. As a result, for spot sizes of 300 µm and larger, the average response duration in dorsal-tOff-αRGCs was >5-fold longer than the average response duration in ventral-tOff-αRGCs (Figure 1E; 1,260 ± 219 ms and 100 ± 29 ms [SEM] for dorsal- and ventral-tOff-αRGCs, respectively, for the 300-µm-diameter spot; 1,245 ± 205 ms and 200 ± 47 ms for dorsal- and ventral-tOff-αRGCs, respectively, for the 800-µm-diameter spot).

Examining the responses of tOff-αRGCs to the stimulus at lower light intensities (mesopic range) revealed that dorsal-tOff-αRGCs increase their response duration with illumination, whereas ventral-tOff-αRGCs display response durations that are independent of light intensity (Figures S1C and S1D).

The large difference we observed in the response durations between dorsal- and ventral-tOff-αRGCs in the photopic range prompted us to examine their morphology to verify that they share similar morphological properties as expected from cells belonging to the same subtype. tOff-αRGCs are predicted to have large dendritic areas, with estimated diameters of around 300 µm [23], and stratify between the two layers of On and Off starburst amacrine cells' processes (called the ChAT bands) just below the Off ChAT band [24–27].

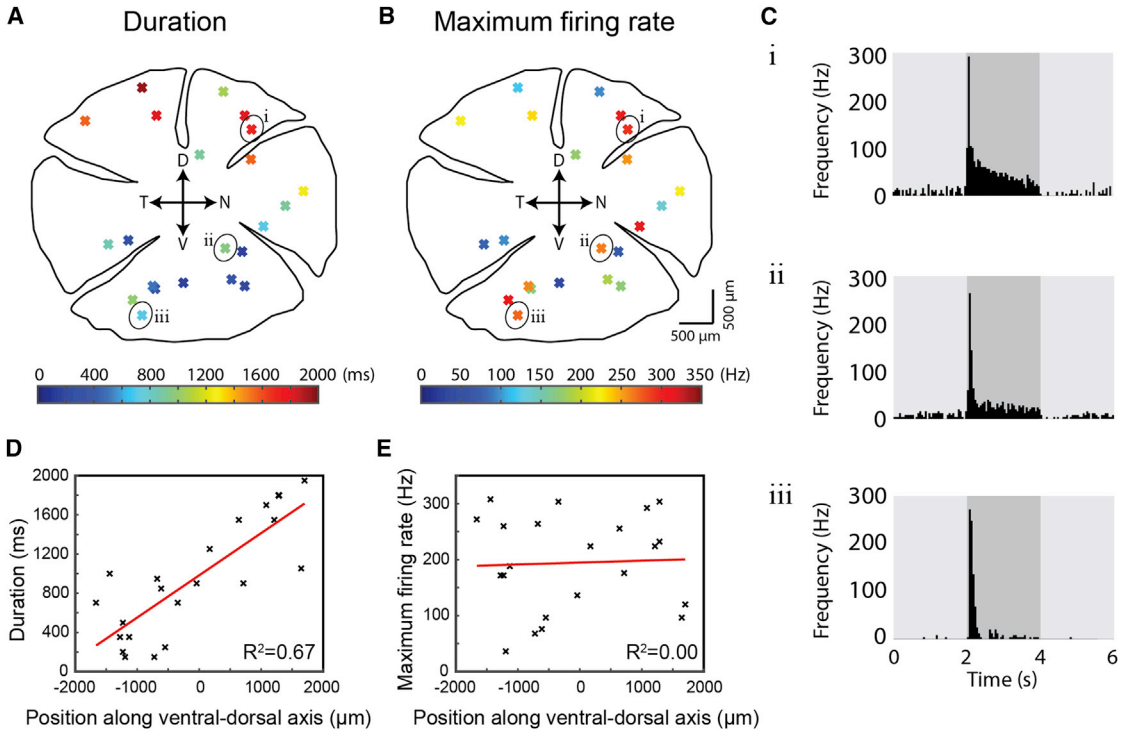

Figure 2. tOff-αRGCs Gradually Change Their Response Properties along the Dorsal-Ventral Axis

(A and B) Positions of 22 tOff-αRGCs recorded from across the retina. Response durations (A) and maximal firing rates (B) to a 400 μm spot are color coded. Cardinal axes are marked in the center. D, dorsal; V, ventral; T, temporal; N, nasal.

(C) PSTHs of 3 representative tOff-αRGCs whose locations are marked in (A) and (B).

(D and E) Plot of response duration (D) and maximal firing rate (E) against position along the ventral-dorsal axis.

In a new set of experiments, a total of 15 GFP+ dorsal RGCs and 17 GFP+ ventral RGCs were filled with CF-594 dye and a proportion of these cells (n = 6 for dorsal and for ventral) were also filled with biocytin to examine their dendrite stratification layers using immunostaining for ChAT bands. The soma sizes and dendritic areas were consistent with them being αRGCs (Figures S2A–S2D), and all examined cells stratified below the Off ChAT band (Figures S2E–S2H), confirming they are indeed tOff-αRGCs. The dendritic areas were slightly smaller for ventral-tOff-αRGCs compared with dorsal-tOff-αRGCs (Figure S2D), which could result from the fact that RGCs are more densely populated in the ventral retina compared with the dorsal retina [28, 29]. Based on their dendritic areas, the estimated diameters for dorsal- and ventral-tOff-αRGCs were 347 ± 8 μm and 320 ± 6 μm (SEM), respectively.

tOff-α RGCs Gradually Change Their Response Properties along the Dorsal-Ventral Axis

In order to understand whether tOff-αRGCs change their response properties gradually along the dorsal-ventral axis or whether there are two distinct populations of tOff-αRGCs (dorsal- and ventral-tOff-αRGCs), we recorded from 22 GFP+ tOff-αRGCs in locations distributed across the entire retina (Figure 2). For these experiments, a single spot size (400 μm dimeter) was used as the light stimulus. Three example tOff-αRGCs located in the dorsal, central, and far ventral retina exhibited long, medium, and short duration responses, respectively (Figure 2C). Plotting response duration against position along dorsal-ventral axis indicated that response duration changes gradually with location (R^2 = 0.67; Figure 2D). No correlation was found between response duration and nasal-temporal location of the cells (R^2 = 0.00). The maximum firing frequency also varied among cells, but as opposed to the gradual change in response duration, firing rate was not correlated to position along the dorsal-ventral axis (R^2 = 0.00; Figures 2B and 2E). This result was independent of baseline activity, as after subtracting the baseline firing rate from the maximum firing rate, still no correlation was found (R^2 = 0.00; data not shown). Particularly, tOff-αRGCs that exhibited similar maximal firing frequencies could display different duration responses depending on their location along the dorsal-ventral axis (Figure 2C).

Dorsal-Ventral Differences Still Exist under Conditions that Preferentially Activate the Ventral Cones

The mouse retina contains two types of cone opsins with different spectral sensitivities: S opsin (short-wavelength or UV light sensitive) and M opsin (mid-wavelength or green light sensitive). While rods' spectral sensitivity is uniform across the entire retina (with peak sensitivity to green light), cones' spectral sensitivity varies along the dorsal-ventral axis due to gradual opsin expression: in the dorsal retina, M opsins dominate, whereas in the ventral retina, S opsins dominate [18–20] (Figure 3A). Could differential cone activation underlie the differences between dorsal- and ventral-tOff-αRGCs? Specifically, the light stimulus

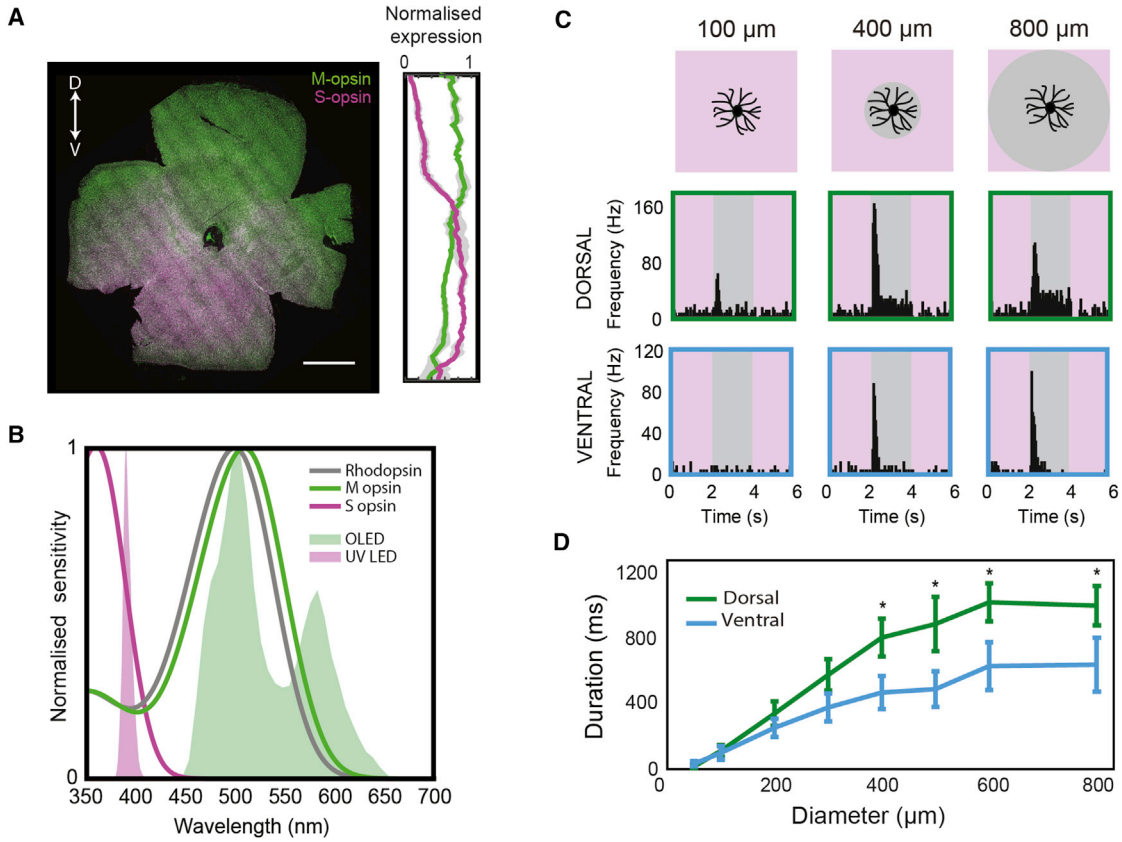

Figure 3. Differential Cone Activation Cannot Explain the Different Length Responses in Dorsal- and Ventral-tOff-αRGCs

(A) Left: an example of a retina immunostained for M (green) and S (magenta) opsin. Double-headed arrow indicates retinal orientation. D, dorsal; V, ventral. Scale bar, 1,000 µm. Right: quantification of relative M and S opsin expression along the dorsal-ventral axis, averaged from three mice.

(B) Graph showing the absorption spectrum for rhodopsin, M and S opsin, and the light spectrum for the organic light-emitting diode (OLED) (white light stimulus used in this study) and the UV LED (used exclusively for this figure).

(C) PSTHs for example dorsal-tOff-αRGC (middle) and ventral-tOff-αRGC (bottom) when a UV light stimulus is used. Top line illustrates the corresponding spot stimuli.

(D) Response duration as a function of spot size for dorsal- and ventral-tOff-αRGCs, when UV light stimulus is used. Error bars represent the mean ± SEM; n = 12 cells from 6 retinas for dorsal; n = 12 cells from 5 retinas for ventral; *p < 0.05 according to Wilcoxon rank-sum test.

used in the experiments described above (Figures 1 and 2) did not contain UV wavelengths and therefore minimally activated S opsins (Figure 3B). As a result, the longer duration responses observed in dorsal-tOff-αRGCs could arise from the greater cone activation in the dorsal retina. To test this, we conducted cell-attached recordings from dorsal- and ventral-tOff-αRGCs in response to a light stimulation consisting of UV light only. Under these conditions, cone activation in the ventral retina is stronger than in the dorsal retina (Figure 3B). Although response durations of dorsal- and ventral-tOff-αRGCs became more similar, we found that, even with a UV light stimulus, dorsal-tOff-αRGCs still exhibited significantly longer response durations than ventral-tOff-αRGCs (Figures 3C and 3D). These experiments did not isolate cones contribution to tOff-αRGCs responses, as the UV light also activates rhodopsin and M opsin due to their beta bands (Figure 3B). Thus, while we could not rule out the possibility that differential cone activation may contribute to the differences in response duration between dorsal- and ventral-tOff-αRGCs, we concluded that additional mechanisms must be involved.

Input from the Primary Rod Pathway Differs between Dorsal- and Ventral-tOff-αRGCs

There is substantial information in the literature on the retinal circuit underlying tOff-αRGC responses [24, 27, 30–34]. In addition to receiving glutamatergic input from Off cone bipolars, tOff-αRGCs also receive input from glycinergic amacrine cells, called AII cells [24, 30, 31]. These AII amacrine cells also regulate the amount of glutamatergic input the tOff-αRGC receives by forming glycinergic synapses with the Off cone bipolars [30, 31]. In order to understand how this circuit differs between dorsal- and ventral-tOff-αRGCs, cell-attached recordings were carried out in the presence of the glycine receptor antagonist, strychnine (1 µM). Under these conditions, input from AII amacrines onto tOff-αRGCs and Off cone bipolars is abolished, and so the remaining light responses of tOff-αRGCs are predicted to be solely the result of glutamatergic input from the Off cone bipolars (Figure 4A). Surprisingly, under glycinergic blockade, dorsal-tOff-αRGCs had short-duration responses similar to ventral-tOff-αRGCs (Figures 4B and 4C). Strychnine did not significantly reduce the response duration for ventral-tOff-αRGCs. In

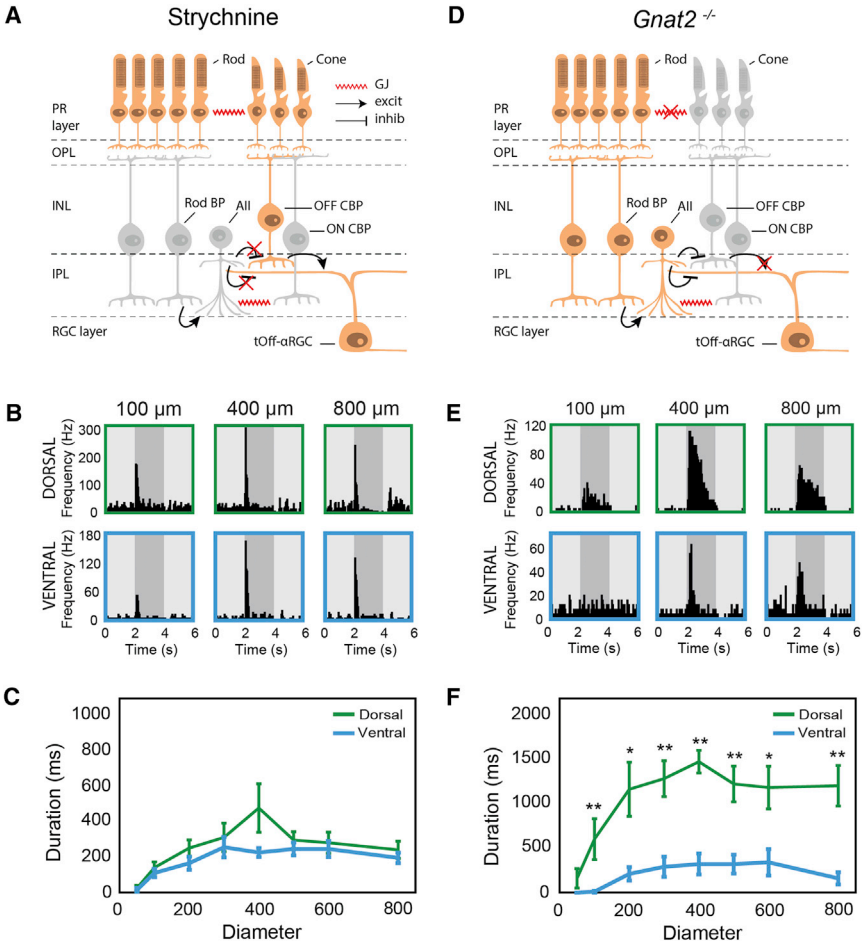

Figure 4. Rod Input Differs between Dorsal- and Ventral-tOff-αRGCs

(A) Diagram illustrating the circuit underlying the response in tOff-αRGCs under pharmacological blockade of glycine. Active pathways are highlighted in orange, inactive in gray.

(B) PSTHs of example dorsal-tOff-αRGC (top) and ventral-tOff-αRGC (bottom) in the presence of the glycine receptor blocker strychnine (1 μM).

(C) Response duration as a function of spot size for dorsal- and ventral-tOff-αRGCs in the presence of strychnine. n = 10 cells from 4 retinas for dorsal; n = 10 cells from 3 retinas for ventral.

(D) Diagram illustrating the circuit underlying the response in tOff-αRGCs in *gnat2*$^{-/-}$ mice. Active pathways are highlighted in orange, inactive in gray.

(E) PSTHs of example dorsal-tOff-αRGC (top) and ventral- tOff-αRGC (bottom) in retinas of *gnat2*$^{-/-}$ mice.

(F) Response duration as a function of spot size for dorsal- and ventral-tOff-αRGCs in retinas of *gnat2*$^{-/-}$ mice. n = 5 cells for each group. Error bars represent the mean ± SEM, *p < 0.05 and **p < 0.01 according to Wilcoxon rank-sum test. PR, photoreceptor; OPL, outer plexiform layer; INL, inner nuclear layer; IPL, inner plexiform layer; BP, bipolar; CBP, cone bipolar; GJ, gap junction; excit, excitation; inhib, inhibition.

See also Figure S3.

addition, we observed no differences between the maximum firing frequencies of dorsal- and ventral-tOff-αRGCs (Figure S3A). Strychnine eliminates all glycinergic inhibition and could potentially reduce response duration in dorsal-tOff-αRGCs via any glycinergic cell. Yet, the most likely amacrine cell to cause the effect is the AII, as it is a primary input neuron to the tOff-αRGC and provides it with direct inhibition [30, 31]. This suggests that the AII amacrine input underlies the difference between dorsal- and ventral-tOff-αRGCs' response durations. However, we do not know whether this is due to differences in intrinsic properties among AIIs or due to differences in their upstream circuits (see Discussion).

To further investigate differential input of AII amacrine cells onto tOff-αRGCs, we carried out cell-attached recordings of dorsal- and ventral-tOff-αRGCs in retinas of *gnat2*$^{-/-}$ mice [35]. These mice lack functional cone photoreceptors, and their secondary rod pathway is abolished [36], so any remaining light responses in tOff-αRGCs would arise solely from the primary rod pathway (Figure 4D) [37]. Dorsal-tOff-αRGCs in *gnat2*$^{-/-}$ retinas exhibited robust, long-duration light responses (Figures 4E, 4F, and S3B). In contrast, ventral-tOff-αRGCs light responses were shorter and had diminished maximal firing frequencies (Figures 4E, 4F, and S3B). Together, our results suggest that the longer response durations in dorsal-tOff-αRGCs are mediated by the primary rod pathway via the AII amacrine cell.

To test how the difference in AII signaling affects response duration of tOff-αRGCs, we conducted whole-cell voltage-clamp recordings in dorsal- and ventral-tOff-αRGCs to assess their excitatory and inhibitory synaptic inputs. AII amacrine cells have a narrow dendritic arbor, but their receptive field size is larger and depends on the AII-AII coupling strength, which is regulated by ambient light [38]. AII amacrine cells mediate tOff-αRGCs response properties both directly via inhibition and indirectly via inhibition of Off cone bipolars that excite them [30, 31]. Indeed, the tOff-αRGC typically receives increased excitation and a simultaneous relief of inhibition at light offset [26, 27, 30]. We therefore hypothesized that both excitatory and disinhibitory synaptic inputs would be more prolonged in dorsal-, but not ventral-, tOff-αRGCs.

Example current traces from dorsal- and ventral-tOff-αRGCs when clamped at holding potentials of 0 and −60 mV can be seen in Figures 5A and 5B, revealing the inhibitory and excitatory synaptic inputs, respectively. By observing the traces for the dorsal-tOff-αRGC, it is apparent that both disinhibition and excitation are composed of a transient and a sustained component (Figure 5A). The transient components were reduced with the 800 μm spot, suggesting that they are susceptible to an inhibitory surround, whereas the sustained components were not. In contrast, disinhibition and excitation appear purely transient for the ventral-tOff-αRGC (Figure 5B). Accordingly, for both disinhibition and excitation, the charge transfer during the 2 s spot presentation was significantly larger for dorsal-tOff-αRGCs compared with ventral-tOff-αRGCs (Figures 5C and 5D). As the

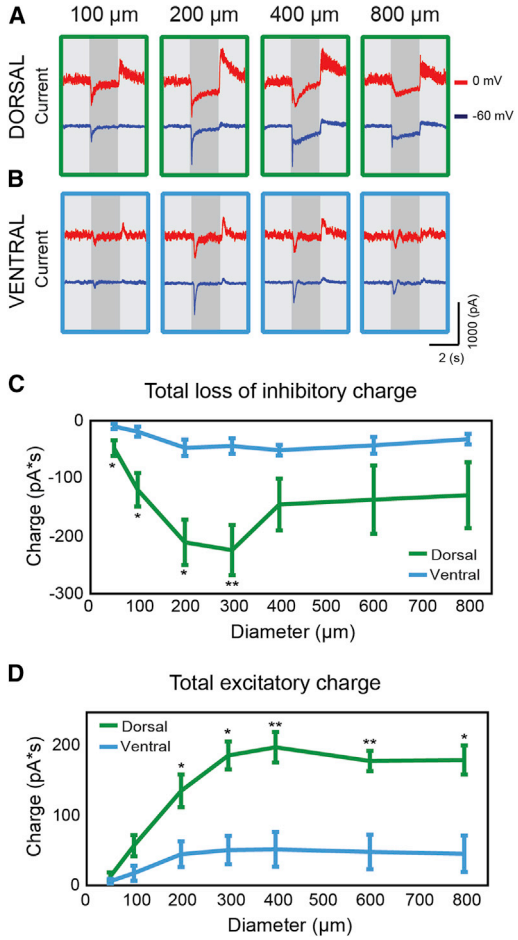

Figure 5. Excitatory and Inhibitory Synaptic Inputs Differ between Dorsal- and Ventral-tOff-αRGCs

(A and B) Current traces of an example dorsal-tOff-αRGC (A) and an example ventral-tOff-αRGC (B) when held at 0 (red) and −60 (blue) mV.

(C and D) Total loss of inhibitory charge (C) and total gain of excitatory charge (D) during the 2 s spot presentation as a function of spot size for dorsal- and ventral-tOff-αRGCs. Error bars represent the mean ± SEM; n = 5 for each group; *p < 0.05 and **p < 0.01 according to Wilcoxon rank-sum test.

sustained disinhibitory and excitatory components in dorsal-tOff-αRGCs had similar temporal and spatial properties, it is likely that they originate from the same source, and as they were absent in the ventral-tOff-αRGC, we can surmise this source to be the AII amacrine.

Wild House Mice Exhibit Similar Dorsal-Ventral Differences in tOff-αRGCs

Most modern laboratory mouse strains were initially generated back in the 1920s–1930s and have been inbred in captivity ever since, for an estimated hundreds of generations [39]. In order to confirm that the differences observed between dorsal- and ventral-tOff-αRGCs are not the result of excessive inbreeding or specific to our laboratory strain, we examined retinas of wild house mice (wild mice) that were trapped in fields and kept under laboratory conditions for a maximum of ten generations (see STAR Methods).

Similar to the *Calb2-EGFP* mice, wild mice exhibited a gradient expression of M and S opsins (Figures 6A and 6B). However, unlike the *Calb2-EGFP* mouse, not all wild mice had an even distribution of cone photoreceptors. Interestingly, in 8/15 mice examined, cones in the ventral retina appeared in an organized mosaic of high-density cone clusters (Figures 6B, S4A, and S4B). For simplicity, only data recorded from retinas that exhibited these cone clusters were used in the analysis below. Despite these differences in cone photoreceptor distribution, dorsal- and ventral-tOff-αRGCs in wild mice exhibited differences in their spiking activities, similar to the differences detected in retinas of *Calb2-EGFP* mice (Figure 6). In these experiments on wild retinas, cells were patched blindly by targeting large somas. To verify that the cells we recorded from were indeed tOff-αRGCs, each recorded cell was filled with CF-594 dye and biocytin. A two-photon z stack was taken after recording to confirm that the dendritic field size and morphology matched that of an αRGC [23, 27]. Afterward, the retina was immunostained for ChAT and biocytin to examine the dendrite stratification layer. Only cells whose dendrites stratified below the Off ChAT band were concluded to be tOff-αRGCs [24–27]. Spiking activities of an example dorsal-tOff-αRGC can be seen in Figure 6C, along with its dendritic morphology (Figure 6D) and its stratification pattern (Figure 6E). An example ventral-tOff-αRGC can be seen in Figures 6F–6H. In retinas from wild mice, dorsal-tOff-αRGCs (n = 4) had significantly longer response durations than ventral-tOff-αRGCs (n = 6; Figure 6I), although their maximal firing rates remained similar (Figure 6J). We also compared between tOff-αRGCs in the wild and *Calb2-EGFP* mice and found that, although there was no statistically significant difference between ventral-tOff-αRGCs, dorsal-tOff-αRGCs in wild mice were even more sustained than those in the *Calb2-EGFP* mice (Figures S4C and S4D). These findings not only confirm that the differences between dorsal- and ventral-tOff-αRGCs are not restricted to our specific laboratory mouse line but also suggest that they may have a functional role in mouse vision.

DISCUSSION

In this study, we demonstrated that cells belonging to a specific RGC subtype can exhibit different response properties according to their location in the retina, as a result of variations in their underlying circuitry. We found that tOff-αRGCs were relatively more sustained in the dorsal retina compared with the ventral retina and that this change was gradual along the dorsal-ventral axis. Experiments using a UV light stimulus excluded the possibility that this was merely due to differential cone activation, as a result of M and S opsins dominating in the dorsal and ventral retina, respectively. Instead, isolating the cone pathway by pharmacologically blocking glycinergic input from the rod pathway revealed similar light responses in dorsal- and ventral-tOff-αRGCs. Furthermore, eliminating the cone circuitry using *gnat2*$^{-/-}$ mice that lack functioning cones revealed robust sustained responses in dorsal-tOff-αRGCs but only diminished responses in ventral-tOff-αRGCs. These data led us to conclude that it is the input from the primary rod pathway via the AII amacrine that differs between dorsal- and ventral-tOff-αRGCs. These differences between dorsal- and ventral-tOff-αRGCs were replicated in retinas of wild mice, confirming they are not

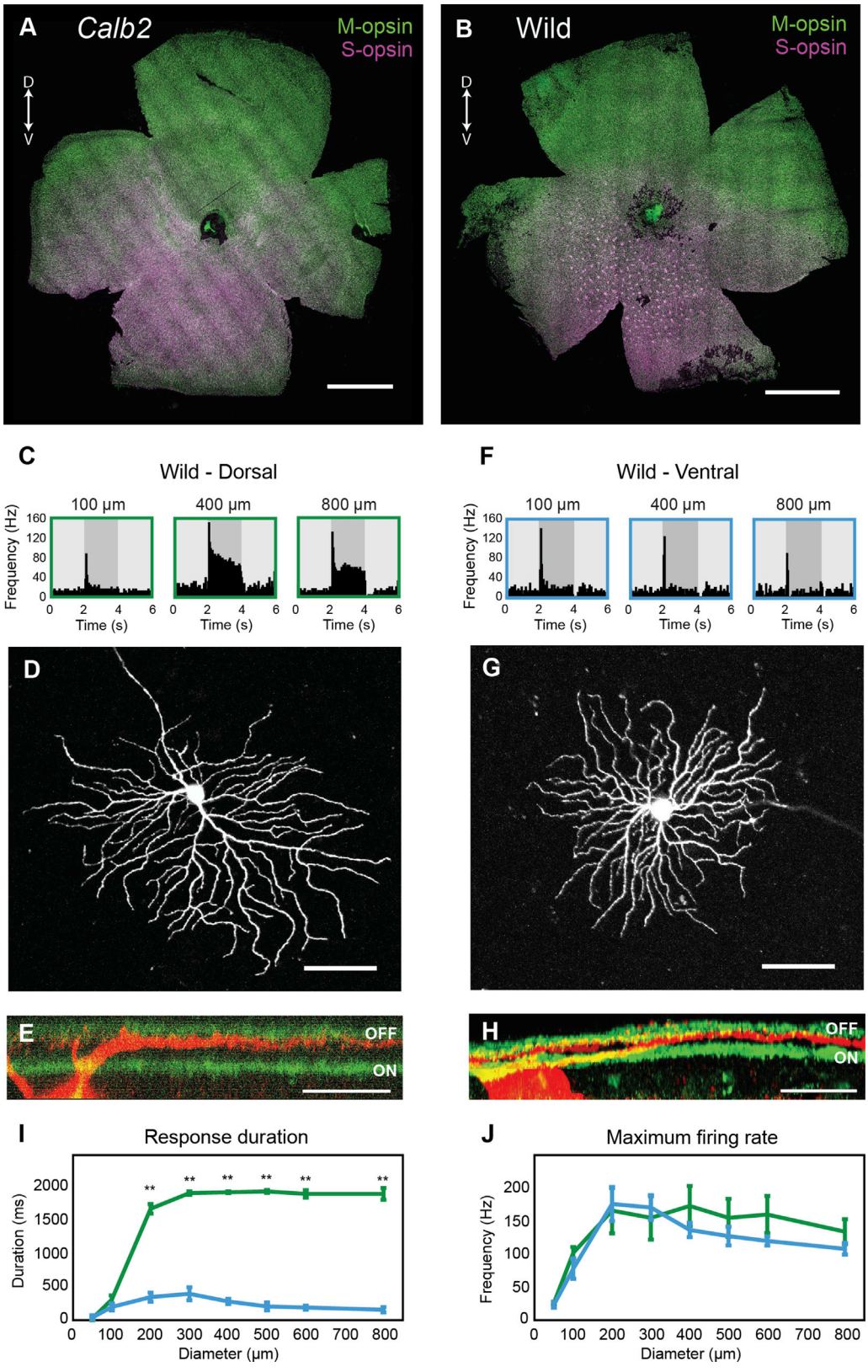

(legend on next page)

the result of inbreeding and suggesting that they actually pose some visual advantage to the mouse.

The finding that tOff-αRGCs display location-dependent response properties was facilitated by the use of a transgenic mouse line that specifically labels tOff-αRGCs [22]. Indeed, the use of other transgenic mouse lines and the recent advancements in imaging and recording techniques has enabled a number of new retina discoveries, including the existence of new RGC types, and among them the transient On-αRGC [5, 40]. Other factors enabling our findings were the use of the light in the photopic range and the relatively long duration stimuli, which made it possible to detect long-duration responses. Indeed, the difference in response durations between dorsal- and ventral-tOff-αRGCs was most apparent at photopic light levels (Figures S1C and S1D). Although the original study in which the mouse line was characterized reported on homogeneous responses of tOff-αRGCs [22], we believe this resulted from recordings that are restricted to a specific retinal area. Indeed, another study showed that tOff-αRGCs display a wide range of response durations under high mesopic illumination [41].

While we hypothesize that the prolonged response in dorsal-tOff-αRGCs is beneficial for mouse vision, this prolonged response emerges only in high mesopic intensities and is strengthened in photopic intensities. Our study adds to previous studies showing that the visual information carried by RGCs may be fundamentally different at low- and high-light levels. For example, receptive field center-surround organization of RGCs changes with light levels, as antagonistic surround weakens or is even abolished as light level decreases [42–44]. In another example, On-αRGCs change their spatial integration from linear to non-linear as light levels increase [45]. Both minimal surrounds and linear summation at low light levels enhance spatial averaging to increase sensitivity to weak inputs, while at high light levels, RGCs' receptive fields sharpen to increase selectivity for small versus large stimuli. Overall, this suggests a unifying principle that encoding of the fine spatial details in the environment is improved as light conditions allow it.

Although the experiments using strychnine and *gnat2*$^{-/-}$ mice led us to conclude that the difference between dorsal- and ventral-tOff-αRGCs is due to differential input from the primary rod pathway, we do not know where in this pathway the difference originates. In the mouse, rod distribution is uniform across the retina [46], suggesting that the difference originates further along the primary rod pathway, either with the rod bipolars, the AII amacrines, or their synaptic connections. It remains for future investigation to determine whether other RGC subtypes, besides the tOff-αRGC, also receive less input from the primary rod pathway in the ventral retina. Such a differential input may cause additional RGCs to display a qualitative difference in their light responses along the dorsal-ventral axis.

As the mouse retina lacks a fovea or area centralis, it has until recently been considered uniform, and as such, defining RGC subtypes has been fairly straightforward. RGC subtypes are defined by sharing the same morphology, function, and by forming a mosaic. Our findings challenge this method of classification, as we show that cells within a given RGC subtype may exhibit functional variations based on their location. Previous studies challenged the mosaic requirement for defining a RGC subtype, showing that a number of RGC subtypes are non-uniformly distributed across the retina. W3 RGCs (presumed local edge detector), M1 and M2 RGCs (intrinsically photosensitive), F-RGCs, and On-αRGCs all display non-uniform densities, which change with retinal location [28, 47–49]. Finally, another study revealed a RGC subtype whose dendritic morphology differed in the outermost ventral region of the retina, challenging the morphology requirement for defining a RGC subtype [50]. Taken together, these studies question the current method of RGC subtype classification. Moreover, they suggest that, when studying a specific cell type or population neuronal activity, one should carefully consider not only the precise experimental conditions but also the exact location of recordings.

In primates and carnivores that have specialized areas for high acuity vision, RGCs show a non-uniform distribution in the retina, as their density increases and dendritic arbor size decreases toward the fovea or area centralis [51, 52]. This heterogeneity is not unique to RGCs, as bipolar cells jointly scale with RGCs toward areas of peak density [53, 54]. This is different in mouse, as On-αRGCs change their dendritic arbor size with retinal location, but bipolar cells that innervate them do not scale their axonal arbor proportionally [28]. Recent evidence reveals that heterogeneity in the primate retina is also evident at the functional level, as visual processing and circuitry of midget RGCs differ between fovea and periphery [55]. Thus, retinal circuits of various mammalian species display specialized computations that are adjusted to the visual demands.

In addition to the locational differences observed in RGCs, several other lines of evidence suggest that the mouse retina is not uniform and that the ventral retina may have a function distinct from the dorsal retina. First, RGCs are more densely populated in the ventral retina [28, 29]. This was in agreement with our finding that ventral-tOff-αRGCs had slightly smaller dendritic fields than dorsal-tOff-αRGCs (Figure S2D). Second, in the ventral retina, two opsins (M and S) are expressed, as opposed to one (M) opsin, which dominates in the dorsal retina [18–20]

Figure 6. Wild Mice Exhibit Dorsal-Ventral Differences in tOff-αRGCs Response Durations that Are Similar to *Calb2-EGFP* Mice

(A and B) *Calb2-EGFP* retina (A, same as Figure 3A,) and a wild mouse retina (B) immunostained for M (green) and S (magenta) opsin. Double-headed arrow indicates retinal orientation. D, dorsal; V, ventral. Scale bar, 1,000 μm.

(C–J) Response properties and morphologies of tOff-αRGCs in wild retinas.

(C and F) PSTHs of an example dorsal-tOff-αRGC (C) and an example ventral-tOff-αRGC (F) in a wild retina.

(D and G) Two-photon z projection of dorsal (D) and ventral (G) example cells whose light responses are depicted in (C) and (F), correspondingly. Scale bar, 100 μm.

(E and H) Stratification pattern of dorsal (E) and ventral (H) example cells whose light responses are depicted in (C) and (F), correspondingly. Scale bar, 25 μm. "OFF" and "ON" indicate Off and On ChAT bands (green).

(I and J) Response durations (I) and maximal firing rates (J) as a function of spot size for dorsal- and ventral-tOff-αRGCs in wild retinas. Error bars represent the mean ± SEM; n = 4 for dorsal-tOff-αRGCs; n = 6 for ventral-tOff-αRGCs; **$p < 0.01$ according to Wilcoxon rank-sum test.

See also Figure S4.

(Figure 3A). Although several explanations have been put forward with regards to the role of UV sensitive (S) opsins in the ventral retina [19, 56], there has been no consensus. A simple explanation is that by expressing two opsins, UV (S) and green (M) sensitive, the spectral range is extended, increasing visual sensitivity in the ventral retina [57]. Third, in half of the wild mice, we observed an organized mosaic of high-density cone clusters in the ventral retina (Figures 6B and S4B). While the function of these cone clusters is outside the scope of this paper, it is further evidence that the ventral retina may have some specialized function.

Like mice, rats have laterally facing eyes, panoramic vision, and lack retinal specializations, such as fovea or area centralis. Tracking rats' eye movements revealed that while the left and right eyes act independently during movement, they image a continuous overhead binocular field [58]. If the same is true for the mouse, the ventral specializations may result from this unique representation of the overhead field. In rats, projecting a visual stimulus above the animal onto their binocular field, and thereby activating the ventral retina, elicited a flight response. However, when the same visual stimulus was projected to the side or in front of the animal, no flight response was observed [58]. When a similar experiment was conducted in mice, the same behavioral pattern was observed [59]. This suggests that the same visual stimulus may be processed differently depending on the retinal area it is perceived by. Our observation that dorsal- and ventral-tOff-αRGCs display different response properties fits very well with this theory. One possible explanation to the difference in response durations could be the following: as ventral-tOff-αRGCs report on the presence of predators above, a short response is sufficient to alert the mouse. Meanwhile, as dorsal-tOff-αRGCs report on activity at ground level, such as varied terrain and food availability, a prolonged response could better represent the scene (assuming rate coding occurs in post-synaptic targets), as the high continuous discharge can be temporarily modified either to be increased or decreased. Because tOff-αRGCs have low spontaneous firing rates [26, 27], purely transient cells (ventral-tOff-αRGCs) would report on the visual scene primarily by increasing their firing rate, while little information can be provided by decreasing their firing rate, as it cannot go below zero. Thus, we hypothesize that RGC response properties change with retinal location, not only to better sample the mouse's visual image, which naturally differs between the upper and lower fields, but also to meet the different functional demands placed on the two retina halves.

STAR★METHODS

Detailed methods are provided in the online version of this paper and include the following:

- KEY RESOURCES TABLE
- CONTACT FOR REAGENT AND RESOURCE SHARING
- EXPERIMENTAL MODEL AND SUBJECT DETAILS
  - Animals
- METHOD DETAILS
  - Tissue preparation
  - Electrophysiology
  - Light stimuli
  - Intracellular filling and immunofluorescence
- QUANTIFICATION AND STATISTICAL ANALYSIS
  - Data analysis
  - Statistical analysis
- DATA AND SOFTWARE AVAILABILITY

SUPPLEMENTAL INFORMATION

Supplemental Information includes four figures and can be found with this article online at https://doi.org/10.1016/j.cub.2018.01.016.

ACKNOWLEDGMENTS

We thank Prof. Tali Kimchi (Weizmann Institute of Science) for the supply of wild house mice and Dr. Roy Harpaz and Dr. Ariel Goldstein for statistical advice. We thank Prof. Michal Schwartz, Prof. Ilan Lampl, Prof. Tali Kimchi, and the Rivlin lab for reading and commenting on the manuscript. This project has received funding from the I-CORE (51/11), the Minerva Foundation, the ISF Foundation (1396/15), the European Research Council under the European Union's Horizon 2020 research and innovation program (grant agreement no. 757732), Dr. and Mrs. Alan Leshner, the Lubin-Schupf Fund for Women in Science, the Charles and David Wolfson Charitable Trust, and Ms. Lois Pope. R.A.W. was supported by the Dean of Faculty fellowship at Weizmann Institute of Science. M.R.-E. is incumbent of the Sara Lee Schupf Family Chair.

AUTHOR CONTRIBUTIONS

R.A.W. designed and conducted experiments, analyzed and interpreted the results, and wrote the paper. N.S. assisted with cell fill experiments. A.G. designed the UV stimulus path. N.K. maintained the mouse colonies and performed genotyping. M.R.-E. designed the experiments, interpreted the results, and wrote the paper.

Received: November 6, 2017
Revised: December 12, 2017
Accepted: January 8, 2018
Published: February 15, 2018

REFERENCES

1. Masland, R.H. (2012). The neuronal organization of the retina. Neuron *76*, 266–280.
2. Masland, R.H. (2001). The fundamental plan of the retina. Nat. Neurosci. *4*, 877–886.
3. Wässle, H. (2004). Parallel processing in the mammalian retina. Nat. Rev. Neurosci. *5*, 747–757.
4. Kuffler, S.W. (1953). Discharge patterns and functional organization of mammalian retina. J. Neurophysiol. *16*, 37–68.
5. Baden, T., Berens, P., Franke, K., Román Rosón, M., Bethge, M., and Euler, T. (2016). The functional diversity of retinal ganglion cells in the mouse. Nature *529*, 345–350.
6. Barlow, H.B., Hill, R.M., and Levick, W.R. (1964). Retinal ganglion cells responding selectively to direction and speed of image motion in the rabbit. J. Physiol. *173*, 377–407.
7. Caldwell, J.H., and Daw, N.W. (1978). New properties of rabbit retinal ganglion cells. J. Physiol. *276*, 257–276.
8. Cleland, B.G., and Levick, W.R. (1974). Properties of rarely encountered types of ganglion cells in the cat's retina and an overall classification. J. Physiol. *240*, 457–492.
9. Farrow, K., and Masland, R.H. (2011). Physiological clustering of visual channels in the mouse retina. J. Neurophysiol. *105*, 1516–1530.
10. Zeck, G.M., Xiao, Q., and Masland, R.H. (2005). The spatial filtering properties of local edge detectors and brisk-sustained retinal ganglion cells. Eur. J. Neurosci. *22*, 2016–2026.

11. Coombs, J., van der List, D., Wang, G.Y., and Chalupa, L.M. (2006). Morphological properties of mouse retinal ganglion cells. Neuroscience *140*, 123–136.
12. Kong, J.H., Fish, D.R., Rockhill, R.L., and Masland, R.H. (2005). Diversity of ganglion cells in the mouse retina: unsupervised morphological classification and its limits. J. Comp. Neurol. *489*, 293–310.
13. Devries, S.H., and Baylor, D.A. (1997). Mosaic arrangement of ganglion cell receptive fields in rabbit retina. J. Neurophysiol. *78*, 2048–2060.
14. Field, G.D., Sher, A., Gauthier, J.L., Greschner, M., Shlens, J., Litke, A.M., and Chichilnisky, E.J. (2007). Spatial properties and functional organization of small bistratified ganglion cells in primate retina. J. Neurosci. *27*, 13261–13272.
15. Peichl, L., and Wässle, H. (1979). Size, scatter and coverage of ganglion cell receptive field centres in the cat retina. J. Physiol. *291*, 117–141.
16. Gouras, P., and Ekesten, B. (2004). Why do mice have ultra-violet vision? Exp. Eye Res. *79*, 887–892.
17. Ratliff, C.P., Borghuis, B.G., Kao, Y.H., Sterling, P., and Balasubramanian, V. (2010). Retina is structured to process an excess of darkness in natural scenes. Proc. Natl. Acad. Sci. USA *107*, 17368–17373.
18. Applebury, M.L., Antoch, M.P., Baxter, L.C., Chun, L.L., Falk, J.D., Farhangfar, F., Kage, K., Krzystolik, M.G., Lyass, L.A., and Robbins, J.T. (2000). The murine cone photoreceptor: a single cone type expresses both S and M opsins with retinal spatial patterning. Neuron *27*, 513–523.
19. Baden, T., Schubert, T., Chang, L., Wei, T., Zaichuk, M., Wissinger, B., and Euler, T. (2013). A tale of two retinal domains: near-optimal sampling of achromatic contrasts in natural scenes through asymmetric photoreceptor distribution. Neuron *80*, 1206–1217.
20. Wang, Y.V., Weick, M., and Demb, J.B. (2011). Spectral and temporal sensitivity of cone-mediated responses in mouse retinal ganglion cells. J. Neurosci. *31*, 7670–7681.
21. Chang, L., Breuninger, T., and Euler, T. (2013). Chromatic coding from cone-type unselective circuits in the mouse retina. Neuron *77*, 559–571.
22. Huberman, A.D., Manu, M., Koch, S.M., Susman, M.W., Lutz, A.B., Ullian, E.M., Baccus, S.A., and Barres, B.A. (2008). Architecture and activity-mediated refinement of axonal projections from a mosaic of genetically identified retinal ganglion cells. Neuron *59*, 425–438.
23. Sun, W., Li, N., and He, S. (2002). Large-scale morphological survey of mouse retinal ganglion cells. J. Comp. Neurol. *451*, 115–126.
24. Münch, T.A., da Silveira, R.A., Siegert, S., Viney, T.J., Awatramani, G.B., and Roska, B. (2009). Approach sensitivity in the retina processed by a multifunctional neural circuit. Nat. Neurosci. *12*, 1308–1316.
25. Margolis, D.J., and Detwiler, P.B. (2007). Different mechanisms generate maintained activity in ON and OFF retinal ganglion cells. J. Neurosci. *27*, 5994–6005.
26. Pang, J.J., Gao, F., and Wu, S.M. (2003). Light-evoked excitatory and inhibitory synaptic inputs to ON and OFF alpha ganglion cells in the mouse retina. J. Neurosci. *23*, 6063–6073.
27. van Wyk, M., Wässle, H., and Taylor, W.R. (2009). Receptive field properties of ON- and OFF-ganglion cells in the mouse retina. Vis. Neurosci. *26*, 297–308.
28. Bleckert, A., Schwartz, G.W., Turner, M.H., Rieke, F., and Wong, R.O. (2014). Visual space is represented by nonmatching topographies of distinct mouse retinal ganglion cell types. Curr. Biol. *24*, 310–315.
29. Dräger, U.C., and Olsen, J.F. (1981). Ganglion cell distribution in the retina of the mouse. Invest. Ophthalmol. Vis. Sci. *20*, 285–293.
30. Manookin, M.B., Beaudoin, D.L., Ernst, Z.R., Flagel, L.J., and Demb, J.B. (2008). Disinhibition combines with excitation to extend the operating range of the OFF visual pathway in daylight. J. Neurosci. *28*, 4136–4150.
31. Murphy, G.J., and Rieke, F. (2008). Signals and noise in an inhibitory interneuron diverge to control activity in nearby retinal ganglion cells. Nat. Neurosci. *11*, 318–326.
32. Demb, J.B., and Singer, J.H. (2012). Intrinsic properties and functional circuitry of the AII amacrine cell. Vis. Neurosci. *29*, 51–60.
33. Beaudoin, D.L., Manookin, M.B., and Demb, J.B. (2008). Distinct expressions of contrast gain control in parallel synaptic pathways converging on a retinal ganglion cell. J. Physiol. *586*, 5487–5502.
34. Murphy, G.J., and Rieke, F. (2006). Network variability limits stimulus-evoked spike timing precision in retinal ganglion cells. Neuron *52*, 511–524.
35. Chang, B., Dacey, M.S., Hawes, N.L., Hitchcock, P.F., Milam, A.H., Atmaca-Sonmez, P., Nusinowitz, S., and Heckenlively, J.R. (2006). Cone photoreceptor function loss-3, a novel mouse model of achromatopsia due to a mutation in Gnat2. Invest. Ophthalmol. Vis. Sci. *47*, 5017–5021.
36. Nusinowitz, S., Ridder, W.H., 3rd, and Ramirez, J. (2007). Temporal response properties of the primary and secondary rod-signaling pathways in normal and Gnat2 mutant mice. Exp. Eye Res. *84*, 1104–1114.
37. Völgyi, B., Deans, M.R., Paul, D.L., and Bloomfield, S.A. (2004). Convergence and segregation of the multiple rod pathways in mammalian retina. J. Neurosci. *24*, 11182–11192.
38. Bloomfield, S.A., and Völgyi, B. (2004). Function and plasticity of homologous coupling between AII amacrine cells. Vision Res. *44*, 3297–3306.
39. Mekada, K., Abe, K., Murakami, A., Nakamura, S., Nakata, H., Moriwaki, K., Obata, Y., and Yoshiki, A. (2009). Genetic differences among C57BL/6 substrains. Exp. Anim. *58*, 141–149.
40. Krieger, B., Qiao, M., Rousso, D.L., Sanes, J.R., and Meister, M. (2017). Four alpha ganglion cell types in mouse retina: function, structure, and molecular signatures. PLoS ONE *12*, e0180091.
41. Farrow, K., Teixeira, M., Szikra, T., Viney, T.J., Balint, K., Yonehara, K., and Roska, B. (2013). Ambient illumination toggles a neuronal circuit switch in the retina and visual perception at cone threshold. Neuron *78*, 325–338.
42. Barlow, H.B., Fitzhugh, R., and Kuffler, S.W. (1957). Change of organization in the receptive fields of the cat's retina during dark adaptation. J. Physiol. *137*, 338–354.
43. Muller, J.F., and Dacheux, R.F. (1997). Alpha ganglion cells of the rabbit retina lose antagonistic surround responses under dark adaptation. Vis. Neurosci. *14*, 395–401.
44. Dedek, K., Pandarinath, C., Alam, N.M., Wellershaus, K., Schubert, T., Willecke, K., Prusky, G.T., Weiler, R., and Nirenberg, S. (2008). Ganglion cell adaptability: does the coupling of horizontal cells play a role? PLoS ONE *3*, e1714.
45. Grimes, W.N., Schwartz, G.W., and Rieke, F. (2014). The synaptic and circuit mechanisms underlying a change in spatial encoding in the retina. Neuron *82*, 460–473.
46. Volland, S., Esteve-Rudd, J., Hoo, J., Yee, C., and Williams, D.S. (2015). A comparison of some organizational characteristics of the mouse central retina and the human macula. PLoS ONE *10*, e0125631.
47. Zhang, Y., Kim, I.J., Sanes, J.R., and Meister, M. (2012). The most numerous ganglion cell type of the mouse retina is a selective feature detector. Proc. Natl. Acad. Sci. USA *109*, E2391–E2398.
48. Hughes, S., Watson, T.S., Foster, R.G., Peirson, S.N., and Hankins, M.W. (2013). Nonuniform distribution and spectral tuning of photosensitive retinal ganglion cells of the mouse retina. Curr. Biol. *23*, 1696–1701.
49. Rousso, D.L., Qiao, M., Kagan, R.D., Yamagata, M., Palmiter, R.D., and Sanes, J.R. (2016). Two pairs of ON and OFF retinal ganglion cells are defined by intersectional patterns of transcription factor expression. Cell Rep. *15*, 1930–1944.
50. Kim, I.J., Zhang, Y., Yamagata, M., Meister, M., and Sanes, J.R. (2008). Molecular identification of a retinal cell type that responds to upward motion. Nature *452*, 478–482.
51. Dacey, D.M. (1993). The mosaic of midget ganglion cells in the human retina. J. Neurosci. *13*, 5334–5355.
52. Dacey, D.M. (1994). Physiology, morphology and spatial densities of identified ganglion cell types in primate retina. Ciba Found. Symp. *184*, 12–28.
53. Wässle, H., and Boycott, B.B. (1991). Functional architecture of the mammalian retina. Physiol. Rev. *71*, 447–480.

54. Chan, T.L., Martin, P.R., Clunas, N., and Grünert, U. (2001). Bipolar cell diversity in the primate retina: morphologic and immunocytochemical analysis of a new world monkey, the marmoset Callithrix jacchus. J. Comp. Neurol. *437*, 219–239.

55. Sinha, R., Hoon, M., Baudin, J., Okawa, H., Wong, R.O.L., and Rieke, F. (2017). Cellular and circuit mechanisms shaping the perceptual properties of the primate fovea. Cell *168*, 413–426.e12.

56. Joesch, M., and Meister, M. (2016). A neuronal circuit for colour vision based on rod-cone opponency. Nature *532*, 236–239.

57. Tovée, M.J. (1995). Ultra-violet photoreceptors in the animal kingdom: their distribution and function. Trends Ecol. Evol. *10*, 455–460.

58. Wallace, D.J., Greenberg, D.S., Sawinski, J., Rulla, S., Notaro, G., and Kerr, J.N. (2013). Rats maintain an overhead binocular field at the expense of constant fusion. Nature *498*, 65–69.

59. Yilmaz, M., and Meister, M. (2013). Rapid innate defensive responses of mice to looming visual stimuli. Curr. Biol. *23*, 2011–2015.

60. Gong, S., Zheng, C., Doughty, M.L., Losos, K., Didkovsky, N., Schambra, U.B., Nowak, N.J., Joyner, A., Leblanc, G., Hatten, M.E., and Heintz, N. (2003). A gene expression atlas of the central nervous system based on bacterial artificial chromosomes. Nature *425*, 917–925.

61. Chalfin, L., Dayan, M., Levy, D.R., Austad, S.N., Miller, R.A., Iraqi, F.A., Dulac, C., and Kimchi, T. (2014). Mapping ecologically relevant social behaviours by gene knockout in wild mice. Nat. Commun. *5*, 4569.

62. Wei, W., Elstrott, J., and Feller, M.B. (2010). Two-photon targeted recording of GFP-expressing neurons for light responses and live-cell imaging in the mouse retina. Nat. Protoc. *5*, 1347–1352.

63. Ivanova, E., Toychiev, A.H., Yee, C.W., and Sagdullaev, B.T. (2013). Optimized protocol for retinal wholemount preparation for imaging and immunohistochemistry. J. Vis. Exp. e51018.

64. Rivlin-Etzion, M., Zhou, K., Wei, W., Elstrott, J., Nguyen, P.L., Barres, B.A., Huberman, A.D., and Feller, M.B. (2011). Transgenic mice reveal unexpected diversity of on-off direction-selective retinal ganglion cell subtypes and brain structures involved in motion processing. J. Neurosci. *31*, 8760–8769.

65. Brainard, D.H. (1997). The psychophysics toolbox. Spat. Vis. *10*, 433–436.

66. Pelli, D.G. (1997). The VideoToolbox software for visual psychophysics: transforming numbers into movies. Spat. Vis. *10*, 437–442.

67. Borghuis, B.G., Marvin, J.S., Looger, L.L., and Demb, J.B. (2013). Two-photon imaging of nonlinear glutamate release dynamics at bipolar cell synapses in the mouse retina. J. Neurosci. *33*, 10972–10985.

Please cite this article in press as: Warwick et al., Inhomogeneous Encoding of the Visual Field in the Mouse Retina, Current Biology (2018), https://doi.org/10.1016/j.cub.2018.01.016

STAR★METHODS

KEY RESOURCES TABLE

REAGENT or RESOURCE	SOURCE	IDENTIFIER
Antibodies		
Anti-Vesicular Acetylcholine Transporter (VAChT)	Millipore	Cat# ABN100; RRID:AB_2630394
Anti-Opsin, Red/Green antibody	Millipore	Cat# AB5405; RRID:AB_177456
OPN1SW (N-20) antibody	Santa Cruz Biotechnology	Cat# sc-14363; RRID:AB_2158332
Alexa Fluor 647-AffiniPure Donkey Anti-Goat IgG (H+L) antibody	Jackson ImmunoResearch Labs	Cat# 705-605-147; RRID:AB_2340437
Alexa Fluor 488-AffiniPure Donkey Anti-Goat IgG (H+L) antibody	Jackson ImmunoResearch Labs	Cat# 705-545-147; RRID:AB_2336933
Donkey Anti-Rabbit IgG (H+L) Antibody, Alexa Fluor 488	Molecular Probes	Cat# A-21206; RRID:AB_141708
Streptavidin Alexa Fluor 594 conjugate	Thermo Fisher Scientific	Cat# S-11227; RRID:AB_2313574
Chemicals, Peptides, and Recombinant Proteins		
Biocytin	Sigma-Aldrich	Cat# B4261
Strychnine hydrochloride	Tocris	Cat# 2785
CF^{TM} 594	Sigma-Aldrich	Cat# SCJ4600029
Experimental Models: Organisms/Strains		
Calb2-EGFP mice	MMRRC	https://www.mmrrc.org/catalog/sds.php?mmrrc_id=283
Software and Algorithms		
ZEN software	Carl Zeiss	https://www.zeiss.com/microscopy/int/products/microscope-software/zen.html
MATLAB	MathWorks	https://www.mathworks.com/products/matlab.html
pCLAMP 10	Molecular Devices	https://de.moleculardevices.com/systems/conventional-patch-clamp/pclamp-10-software
ImageJ	NIH	https://imagej.nih.gov/ij
Psychtoolbox-3	N/A	http://psychtoolbox.org/

CONTACT FOR REAGENT AND RESOURCE SHARING

Further information and requests for resources should be directed to the Lead Contact, Michal Rivlin-Etzion (michal.rivlin@weizmann.ac.il).

EXPERIMENTAL MODEL AND SUBJECT DETAILS

Animals

Calb2-EGFP mice, in which tOff-αRGCs express GFP, were obtained from Mutant Mouse Regional Resource Centers (https://www.mmrrc.org/catalog/sds.php?mmrrc_id=283) [22, 60] and crossed to C57BL/6. The percentage of labeled tOff-αRGCs varied between the mice, and while some showed a mosaic of tOff-αRGCs others labeled only a portion of them. *Gnat2*$^{-/-}$ mice have no functional cones due to a mutation in the cone transducin subunit gene [35]. These mice were on a C57BL/6 background, and crossed with *Calb2-EGFP*. *Gnat2*$^{-/-}$ mice were obtained from Prof. Jeannie Chen at the University of Southern California. Wild house mice, obtained from Prof. Tali Kimchi at the Weizmann Institute of Science [61], were trapped in fields (Idaho, USA) near livestock barns and kept under laboratory conditions for ten generations as an outbred stock of pathogen-free wild mice. Mice were kept on a 12:12 h light-dark cycle with free access to food and water. Mice of either sex were used. All experimental procedures were approved by the Institutional Animal Care and Use Committee (IACUC) at the Weizmann Institute of Science.

METHOD DETAILS

Tissue preparation

Mice (4-6 weeks old) were deeply anesthetized with isoflurane and decapitated. Retinas were isolated under dim red and infra-red (IR) illumination in oxygenated Ames' medium (Sigma, St. Louis, MO, USA). The orientation of the retinas was based on landmarks in

the choroid, as previously described [62]. For experiments in which cells were either recorded in the dorsal or ventral retina, the retinas were cut into dorsal and ventral halves, isolated from the pigment epithelium and mounted photoreceptor side down over a hole of 1–1.5 mm^2 on filter paper, centered over the retina piece (GSWP01300, Merck Millipore, Billerica, MA, USA). Retinas were kept in the dark at room temperature in Ames' medium bubbled with 95% O_2/5% CO_2 until use (maximum 5 h). For experiments in which cells were recoded from various locations across the retina, whole retinas were mounted onto a hydrophilized PTFE membrane insert (PICM01250, Merck Millipore) as described [63].

Electrophysiology

Retinas were placed under a two-photon microscope (Bruker, Billerica, MA, USA) equipped with a Mai-Tai laser (Spectra-physics, Santa Clara, CA USA) and superfused with oxygenated Ames medium at 32-34°C. Identification of and recording from GFP+ cells was carried out as previously described [62, 64]. In short, GFP+ cells were identified using the two-photon microscope laser at 920 nm, to avoid bleaching of the photoreceptors. The inner limiting membrane above the targeted cell was dissected under the microscope with a glass electrode using IR illumination.

Loose-patch recordings (holding voltage set to "OFF") were performed with a new glass electrode (3–5 MΩ) filled with Ames' medium. Intracellular voltage-clamp recordings were carried out using glass electrodes (6–8 MΩ) filled with intracellular solution containing (in mM): $CsMeSO_3$ 110, NaCl 2.8, HEPES 20, EGTA 4, TEA-Cl 5, ATP-Mg 4, GTP-Na_3 0.3, $C_4H_8N_3Na_2O_5P$ 10 and $C_{16}H_{27}N_2OBr$ 5; pH7.35. A giga-Ohm seal was obtained before breaking in. Data were acquired at 10 kHz and for whole-cell mode filtered at 2 kHz with a Multiclamp 700B amplifier (Molecular Devices, CA, USA) using pCLAMP 10 recording software and a Digidata 1550 digitizer (Molecular Devices). For experiments in which strychnine was used, strychnine (1 μM; Cat# 2785, Tocris, UK) was added to the Ames solution and perfused for 20 mins prior to recording from tOff-αRGCs.

A maximum of two cells were recorded from each mouse unless specified otherwise.

Light stimuli

Stimuli were generated using MATLAB and the Psychophysics Toolbox [65, 66]. For the non-UV light visual stimuli, a white, monochromatic organic light-emitting display (OLED-XL, 800 × 600 pixel resolution, 85 Hz refresh rate, eMagin, Bellevue, WA, USA) was used. The spectrum of the OLED is provided in Figure 3B. The display image was projected through a 20 × water-immersion objective (UMPLFLN20xW; Olympus, Tokyo, Japan), via the side port of the microscope, centered on the soma of the recorded cell, and focused on the photoreceptor layer. The diameter of the entire display on the retina was 1 mm across. The visual stimulation consisted of gray background for 2 s, followed by the appearance of a black spot on the gray background, which lasted 2 s before the spot disappeared leaving the same gray background for a further 2 s. Weber's contrast for the black spot on the gray background was −0.85. The light intensity of the gray screen was $6.4x10^4$ $R^*rod^{-1}s^{-1}$. For recording in lower light levels, neutral densities 20 and 10 (ThorLabs, Newton, NJ, USA) were added to decrease the light intensity by factors of 10^2 and 10 without affecting the contrast. In Figure 1, we used other visual stimuli that preceded the stimulus used in this paper.

For UV stimuli, a modified projector (M109s DELL, Austin, TX, USA) containing a UV LED (NC4U134A, peak wavelength 385 nm; Nichia, Anan, Japan) was used [67]. The spectrum of the UV light is provided in Figure 3B. The image was projected on to the retina via the microscope's condenser and created on the photoreceptors layer using two converging lenses (LA4372, LA4052; Thorlabs). The cell soma of the recorded cell was positioned in the center of the visual stimulus. The UV background had a light intensity of $2.8x10^4$ $R^*rod^{-1}s^{-1}$. Weber's contrast for the black spot on the UV background was −0.85.

Intracellular filling and immunofluorescence

Individual tOff-αRGCs were injected with the fluorophore CF™ 594 (250 μM, SCJ4600029, Sigma) and biocytin (1.5% w/v, Sigma) in 0.1M Tris-HCl buffer pH 7.4, from sharp glass electrodes (80-200 MΩ) using negative current. Z stacks of the CF™ 594 filled cells were acquired using the two-photon microscope laser at 780 nm, and steps of 0.5 μm.

Following filling of cells, retinas were fixed in 4% paraformaldehyde in 0.1M phosphate buffered saline (PBS) for 1 h, and then washed in PBS (3 times, 20 min). Retinas were blocked in PBS containing 3% bovine serum albumin and 0.3% Triton X-100 for 1 h, room temperature. Next, retinas were incubated in primary antibodies (1:300 goat anti-VChAT, Merck Millipore; 1:200 rabbit anti-opsin, AB5405, Merck Millipore; 1:300 goat anti-OPN1SW, sc-14363, Santa Cruz Biotechnology, Dallas, TX, USA) diluted in blocking solution, overnight at 4°C. Retinas were washed in PBS (3 times, 1 hr) and then incubated with the secondary antibodies (donkey anti-goat Alexa 647, donkey anti-goat Alexa 488, Jackson ImmunoResearch, West Grove, PA, USA, donkey anti-rabbit Alexa 488, Molecular Probes, OR, USA) and streptavidin-Alexa 594 (1:400; Molecular Probes) in PBS overnight at 4°C. Retinas were washed in PBS (3 times, 30 min) and then mounted on glass slides.

Confocal image acquisition was achieved using a laser scanning confocal microscope (Zeiss, Oberkochen, Germany) equipped with 488, 543, and 633 nm laser lines using ZEN software (Zeiss). Z stack images were acquired using a 63x/1.4 Plan Apochromat oil objective with a step size of 0.25 μm. Tiled images of whole retina were acquired using a 20x/1.0 W Plan Apochromat DIC VIS-IR 75 mm objective. Z-projections and 3D images were reconstructed using ImageJ software.

QUANTIFICATION AND STATISTICAL ANALYSIS

Data analysis

Electrophysiological data were analyzed offline. For loose-patch clamp recordings, spike times were extracted after filtration using a 4 pole Butterworth bandpass filter between 80 and 2000 Hz. Peri-stimulus time histograms (PSTHs) of spiking activity were calculated from 5 repeats using a bin width of 50 ms. The background activity was determined based on the 2 s period of initial gray screen in each trial. This provided the mean baseline activity and it's SD. The bin with highest frequency during the black spot stimulus was used to calculate the maximum response. Response durations were defined based on the number of all bins during the black spot stimulus whose value exceeded the mean baseline activity by 3 SDs. For intracellular recordings, traces were averaged across 4 repeats.

Statistical analysis

We used the Wilcoxon rank sum test to compare between dorsal- and ventral cells for each spot size. Statistical significance was accepted at $p < 0.05$. Numerical values are presented at mean ± standard error of mean (SEM).

DATA AND SOFTWARE AVAILABILITY

Data are available on request. Please contact the lead author.